

## **Photo conversion efficiency of CZTS solar cells fabricated using ZnO as a buffer layer**

**A. G. Kannan<sup>\*1</sup>, T. E. Manjulavalli<sup>1\*</sup>, M. Thambidurai<sup>2</sup>**

<sup>1</sup>Department of Physics, NGM College, Pollachi642001, India

<sup>2</sup>School of Electrical and Electronic Engineering, Nanyang Technological University (NTU), Singapore639798

**Abstract :** Quaternary  $\text{Cu}_2\text{ZnSnS}_4$  (CZTS), a P-type semiconducting material with a direct band gap of 1.4 to 1.5 eV and high absorption coefficient ( $10^4 \text{ cm}^{-1}$ ) in the visible range has been considered as an alternative absorber layer in the fabrication of solar cells. ZnO is a wide-gap n-type material, consisting of abundant and nontoxic elements, and is thus expected to be a good substitute for CdS buffer layer in solar cells. In this paper, we report the study of CZTS and ZnO nanoparticles synthesized by solvothermal method. The structural, optical and electrical properties of prepared nanoparticles were studied using X-ray powder diffraction (XRD), Raman analysis, scanning electron microscopy (SEM), UV-vis absorption and J-V Characteristic studies. The device fabrication and conversion efficiency of CZTS/ZnO solar cells are also discussed.

### **Introduction**

$\text{Cu}_2\text{ZnSnS}_4$  (CZTS) has attracted much attention recently owing to its excellent photovoltaic properties such as optimal direct-band gap energy of 1.5 eV for solar cells and high absorption coefficient in the visible region ( $>10^4 \text{ cm}^{-1}$ ). Moreover, CZTS consists of nontoxic and inexpensive elements<sup>[1-7]</sup>. Much research effort has recently been made on CZTS-based solar cells, and a CZTS/CdS heterojunction solar cell with an efficiency of 8.4% has been reported<sup>[8]</sup>. However, since Cd is a highly toxic element, an alternative material is desired for the buffer layer to realize a more environmentally friendly device<sup>[9]</sup>. ZnO a wide-gap (3.37 eV) n-type material, consisting of abundant and nontoxic elements, is found to be an excellent substitute for CdS<sup>[10-12]</sup>. The conversion efficiencies of CZTS/ZnO cells have exceeded 5% but are still lower than those of the best CZTS/CdS cells<sup>[9]</sup>. In order to realize this, we investigated the structural, optical and electrical properties of CZTS, ZnO nanoparticles synthesized by solvothermal method.

### **Experimental**

All chemicals used in the present work are analytical grade reagents and used without any further purification. In a typical procedure, 0.50 mmol of copper acetate ( $\text{Cu}(\text{CH}_3\text{COO})_2$ ), 0.25 mmol of zinc acetate dihydrate ( $\text{Zn}(\text{CH}_3\text{COO})_2 \cdot 2\text{H}_2\text{O}$ ), 0.25 mmol of tin chloride pentahydrate ( $\text{SnCl}_4 \cdot 5\text{H}_2\text{O}$ ), and 1 mmol of thiourea ( $\text{CH}_4\text{N}_2\text{S}$ ) solutions are prepared in ethylene glycol. The solution was stirred continuously until a clear solution is obtained. The solution is then transferred to a Teflon lined autoclave and it was maintained at 180°C for about 6 hours and then air cooled at room temperature. The precipitates were filtered out, washed with distilled water and absolute ethanol. The final products were dried in vacuum at 60°C for three hours.

In a typical procedure, 0.5mmol of zinc acetate [ $\text{Zn}(\text{CH}_3\text{COO})_2$ ] and 1mmol of sodium hydroxide [NaOH] were taken in a beaker and dissolved in ethylene glycol. Then the mixture was stirred continuously to obtain a clear solution. After that, the solution was transferred into a Teflon lined autoclave and it was maintained at  $160^\circ\text{C}$  for about 5 hours and then air cooled at room temperature. The precipitate was filtered out, washed with deionized water and absolute ethanol. The white product was dried at  $60^\circ\text{C}$  for about 3 hours.

The synthesized CZTS and ZnO powders were characterized by X-ray diffraction (XRD) method using Shimadzu XRD-6000 X-ray diffractometer with a  $\text{CuK}\alpha$  radiation ( $\lambda=1.5406 \text{ \AA}$ ). Raman scattering measurements were performed using Horiba JobinYvon HR800 spectrometer. The morphological and compositional analysis of the nanoparticles were carried out using JEOL mode JSM 6390 SEM with EDX and optical studies of the samples were done using Cary 500 UV-Vis Diffuse Reflectance Spectrophotometer.

### Device Fabrication

A typical solar cell configuration of SLG/Mo/CZTS/ZnO/Al:ZnO/Al structure was used in this study. A molybdenum (Mo) back contact with a thickness of  $1 \mu\text{m}$  was deposited on soda-lime glass (SLG) substrate by DC magnetron sputtering. CZTS absorber layer deposited on Mo-coated soda lime glass substrates by doctor-blade technique using the CZTS paste. The ZnO nanoparticles were dispersed thoroughly in toluene and then coated onto SLG/Mo/CZTS substrate by drop casting method. The Al-doped ZnO (Al:ZnO) transparent conducting window layer was formed on top of the n-type ZnO buffer layer by RF sputtering. Aluminum (Al) metal grid of  $1 \mu\text{m}$  thick layer was deposited by thermal evaporation onto the ZnO:Al window layer with a designed shadow mask. The fabricated device had a total area of approximately  $0.45 \text{ cm}^2$  defined by mechanical scribing. J-V characteristics of solar cell device were recorded with a Keithley 6517B Electrometer. The photocurrent was measured by illuminating the samples with white light of intensity  $100 \text{ mW/cm}^2$ .

### Results and discussion

#### XRD analysis

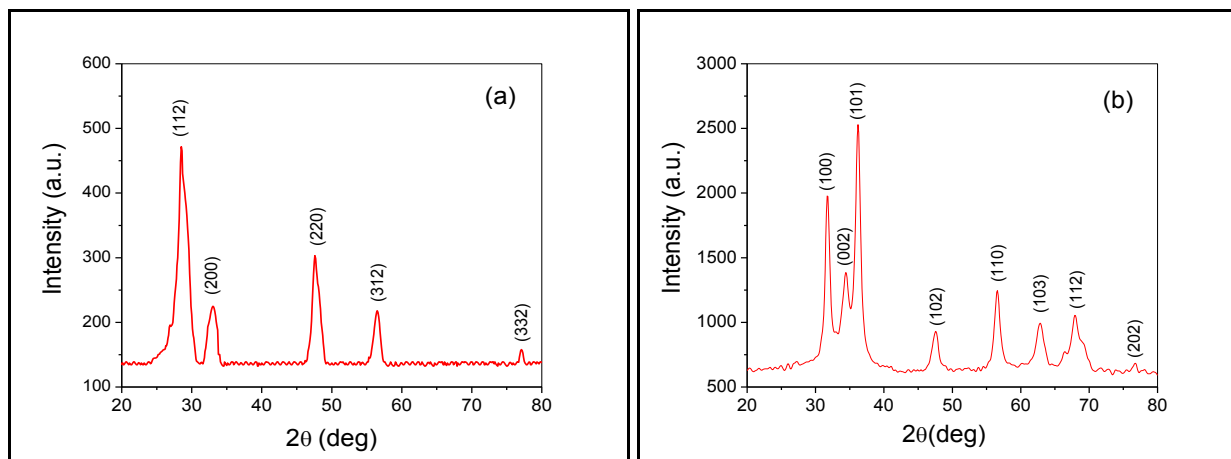


**Fig. 1. XRD spectra of (a) CZTS and (b) ZnO nanoparticles**

Fig.1(a) and 1(b) shows the XRD pattern of CZTS and ZnO nanoparticles. CZTS samples exhibit diffraction peaks corresponding to the (112), (200), (220), (312) and (332) reflection planes of kesterite structure, which is confirmed using standard JCPDS data (Card No. 26-0575). The broadening of the XRD peaks indicates the nanocrystalline nature of the samples. The mean crystallite size  $D$  is determined according to the Scherrer equation  $D = 0.9\lambda / \beta \cos\theta$ , where  $\lambda$  is the X-ray wavelength (for  $\text{CuK}\alpha$  radiation  $\lambda = 1.5406 \text{ \AA}$ ),  $\beta$  is the full width half maximum (FWHM) and  $\theta$  is the diffraction angle. The calculated mean crystallite size is  $7 \text{ nm}$  for CZTS nanoparticles. It is worth mentioning that the calculated lattice constant of CZTS nanoparticles ( $a = 0.5405 \text{ nm}$  and  $c = 1.0871 \text{ nm}$ ), are the same as the value from the standard card ( $a = 0.5427 \text{ nm}$  and  $c = 1.0848 \text{ nm}$ ). Similar results were reported by Mou Pal *et al* <sup>[13]</sup> with the crystallite sizes ranging from  $7.5 \text{ nm}$  to  $10.2 \text{ nm}$  by solvothermal method using ethylenediamine as a solvent.

From the Fig. 1(b), the sharp peaks at scattering angle  $2\theta$  of  $31.71^\circ$ ,  $34.36^\circ$ ,  $36.26^\circ$ ,  $47.38^\circ$ ,  $56.59^\circ$ ,  $62.83^\circ$ ,  $67.89^\circ$  and  $76.69^\circ$  corresponds to the reflection from: (100), (002), (101), (102), (110), (103), (112) and (202) crystal planes, indicating crystalline ZnO with hexagonal wurtzite structure, consistent with the standard JCPDS (Card No.89-0510). No characteristic peaks of impurities could be detected within the precision limit of XRD measurement, which confirms the highly pure and single phase nature of ZnO. The calculated mean crystallite size is 13 nm for ZnO nanoparticles. The calculated lattice constant of ZnO nanoparticles ( $a = 0.3252\text{nm}$  and  $c = 0.5190\text{ nm}$ ), are almost same as the value from the standard card ( $a = 0.3248\text{nm}$  and  $c = 0.5205\text{ nm}$ ). The lattice parameter 'c' was found to be slightly higher than the standard value for ZnO nanoparticles. This may be due to the internal stress in the crystals. Bao *et al* <sup>[14]</sup>, have reported slightly higher 'c' values for ZnO thin films prepared on quartz substrates by a sol-gel method. Y. Zhang *et al* <sup>[15]</sup>, have reported the difference in c-axis lattice parameter and it was attributed to the occurrence of stress in the thin films.

### Raman Analysis

In order to find out the existence of the secondary phase, Raman spectroscopy was performed. Fig. 2(a) and 2(b) shows the Raman Spectra of CZTS and ZnO nanoparticles. Fig. 2(a) shows the Raman spectra of CZTS nanoparticles at the excitation wavelength of 512 nm. It indicates the presence of the two major peaks at  $338\text{ cm}^{-1}$  and  $289\text{ cm}^{-1}$  and is similar to that reported by earlier researchers <sup>[16,17]</sup>. Both these peaks correspond to the CZTS phase. The stronger peaks at  $338\text{ cm}^{-1}$  is due to the  $A_1$  symmetry and it is related with the vibration of the S atoms in CZTS <sup>[18,19]</sup>. Peaks at  $289\text{ cm}^{-1}$  attributes to the vibration of the Zn atoms and S atoms with some contribution from the Cu atoms in CZTS lattice<sup>[20]</sup>. Moreover, it is obvious that there are no extra peaks related to the presence of other compounds such as  $\text{SnS}_2$  ( $314\text{ cm}^{-1}$ ),  $\text{Cu}_2\text{SnS}_3$  ( $352\text{ cm}^{-1}$  and  $374\text{ cm}^{-1}$ ), cubic ZnS ( $352$  and  $275\text{ cm}^{-1}$ ) and orthorhombic  $\text{Cu}_2\text{SnS}_3$  ( $318\text{ cm}^{-1}$ ).

The Raman spectrum of the ZnO nanoparticles at the range of  $200\text{--}800\text{ cm}^{-1}$  is shown in Fig. 2(b). The dominant feature at  $437\text{ cm}^{-1}$  is the result of ZnO nonpolar optical phonons  $E_2$ (high) mode. The  $E_2$ (high) mode corresponds to characteristic band of hexagonal wurtzite phase. The peak located at  $332\text{ cm}^{-1}$  may be attributed to a multiphonon scattering process ( $E_{2H}\text{--}E_{2L}$ ) <sup>[21]</sup>. In addition, the  $E_1$ (LO) peak can also be observed at  $581\text{ cm}^{-1}$ . The appearance of the  $E_1$ (LO) peak is associated with the formation of defects such as oxygen vacancy, zinc interstitial, or their complexes <sup>[22]</sup>.

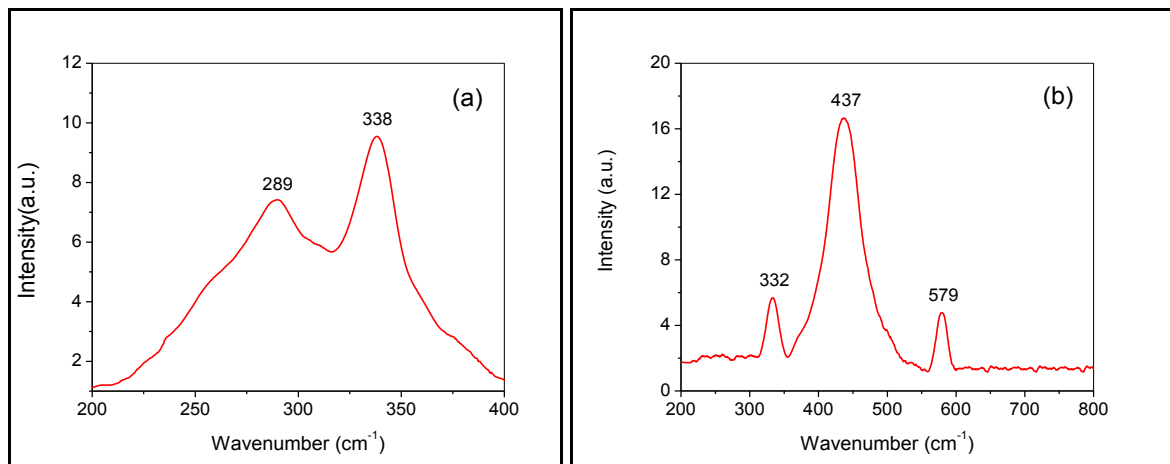


**Fig. 2. Raman spectra of (a) CZTS and (b) ZnO nanoparticles**

### SEM analysis

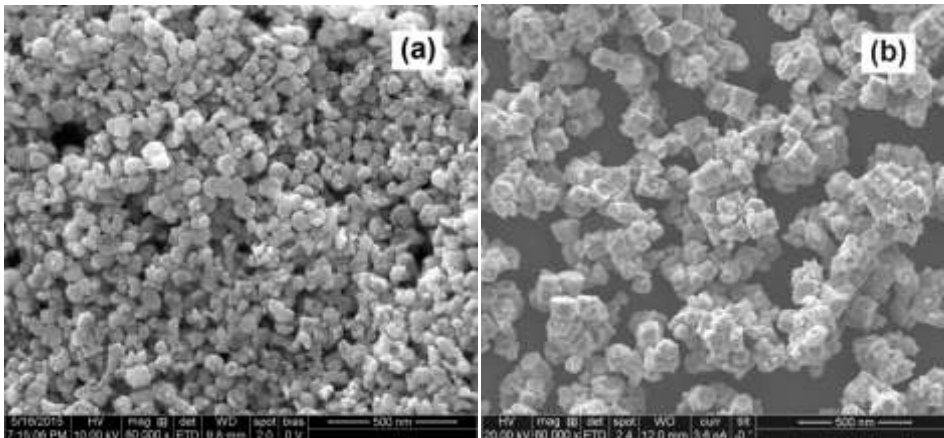


**Fig. 3. SEM Micrographs of (a) CZTS and (b) ZnO nanoparticles**

Fig. 3(a) shows the SEM images of CZTS nanoparticles. The images confirm that the particles are in the nanometer size range. Figure shows that the CZTS samples have nearly uniform monodisperse particles. The scanning electron micrographs of the ZnO nanopowder are shown in Fig.3(b). The ZnO particles were observed to be of uniform size with hexagonal shape.

### Compositional analysis

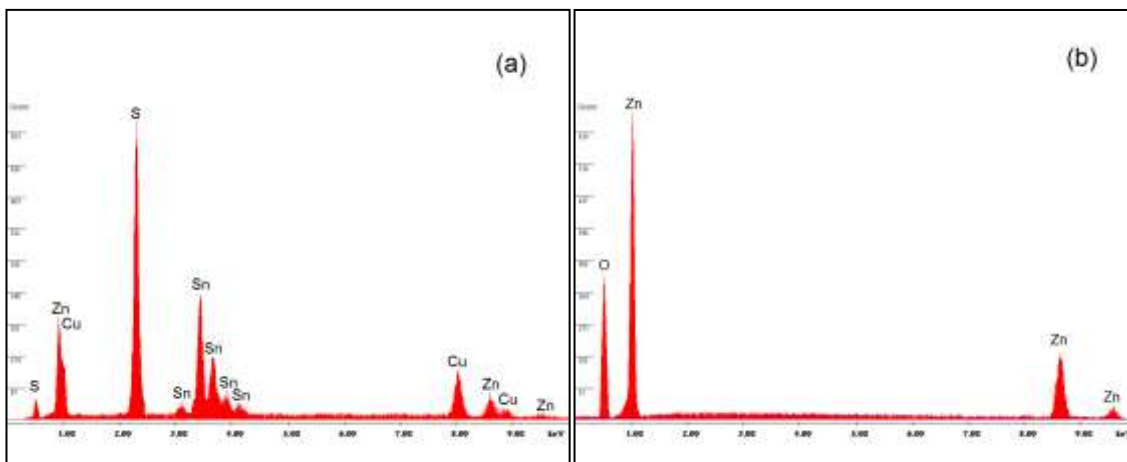
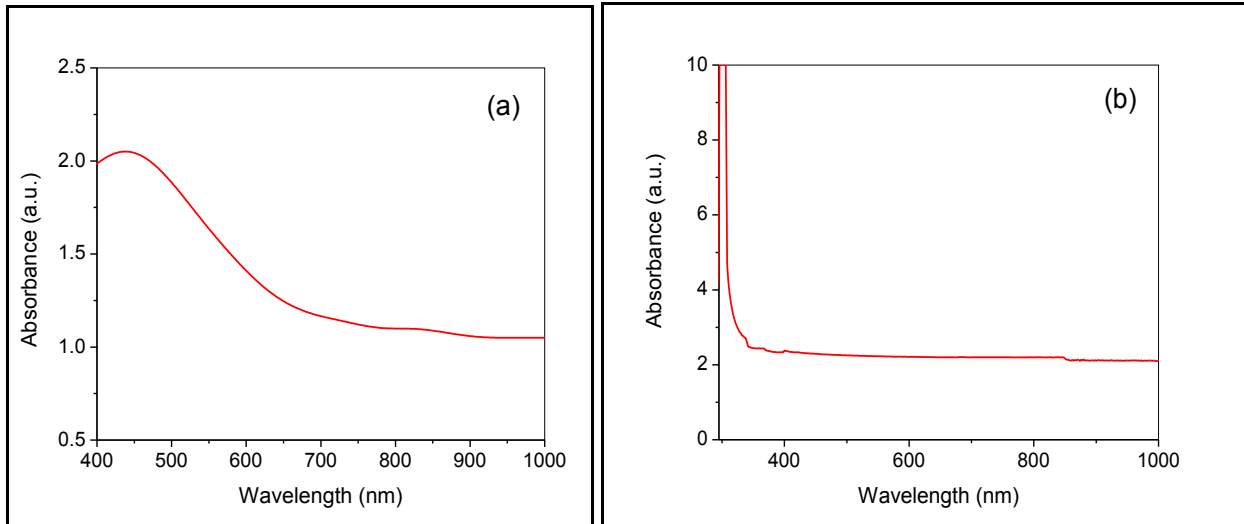


**Fig. 4. EDX spectra of (a) CZTS and (b) ZnO nanoparticles**

The elemental analysis of CZTS and ZnO nanoparticles were carried out by energy dispersive X-ray analysis (EDX) technique. The respective EDX spectra are shown in Fig. 4(a) and 4(b). Fig. 4(a) indicates the presence of copper, zinc, tin and sulfur for the CZTS sample. The stoichiometric ratio of Cu, Zn, Sn and S were computed by integrating the area under each Cu, Zn, Sn and S peak. The EDX spectra of nanoparticles exhibits nearly the stoichiometric composition with atomic percentage of Cu, Zn, Sn and S ratio in the range 24.85 : 12.37 : 12.72 : 50.06 and theoretically expected stoichiometric composition of CZTS (in terms of at %) is Cu : Zn : Sn : S equal to 25.00 : 12.50 : 12.50 : 50.00. Fig. 4(b) indicates the presence of Zinc and Oxygen for the ZnO sample. The average atomic ratio of Zn/O was calculated from the quantification of peaks. Theoretically expected stoichiometry composition of ZnO (in terms of At %) was Zn:O equal to 50.00 : 50.00. The EDX spectra of nanoparticles exhibits nearly the stoichiometric composition with atomic percentage of Zn and O ratio in the range 51.23 : 48.77. EDAX spectrum also reveals that the prepared samples are free from impurities.

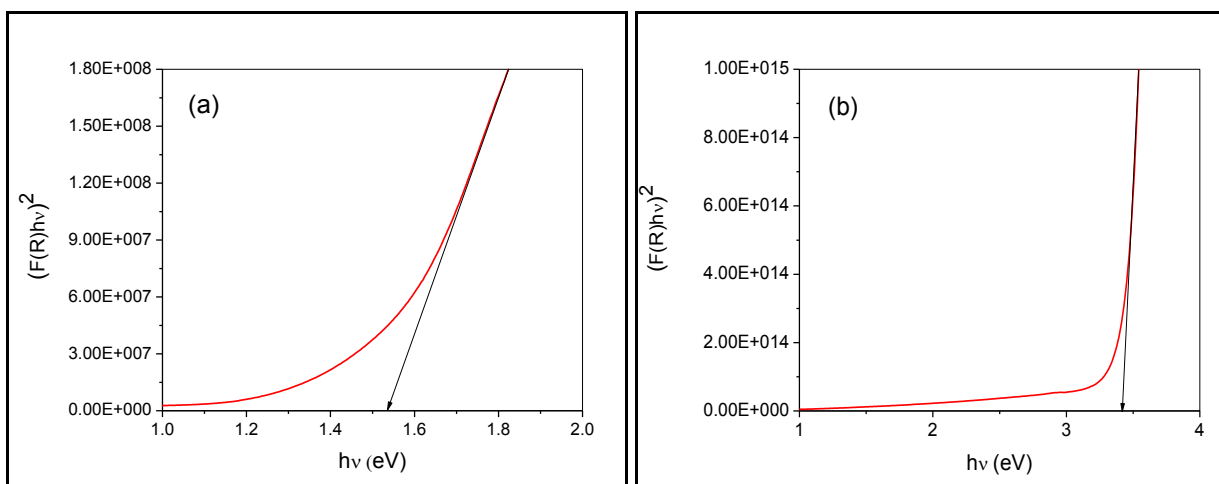
### Optical absorption and band gap

The room temperature UV–vis absorption spectra of CZTS and ZnO samples are shown in Fig. 5(a) and 5(b). The UV–vis absorption spectra of the samples were recorded in diffuse reflectance mode using BaSO<sub>4</sub> as reference. The reflectance values were converted to absorbance by application of the Kubelka-Munk function<sup>[23]</sup>. The Kubelka-Munk formula can be expressed by the relation  $F(R) = (1-R)^2/2R$ , where  $F(R)$  is the Kubelka-Munk function which corresponds to the absorbance and  $R$  is the reflectance (%).



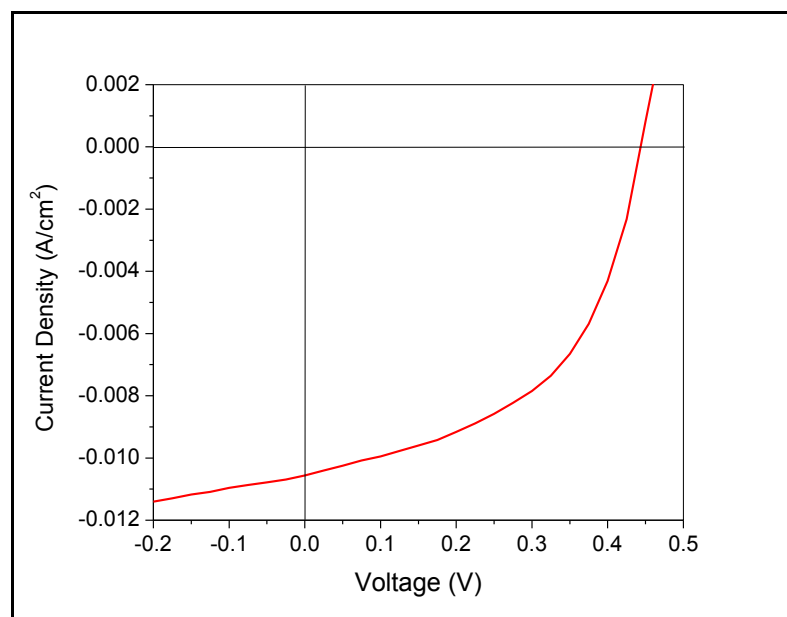
**Fig. 5. UV-absorption spectra of (a) CZTS and (b) ZnO nanoparticles**

Fig. 5(a) exhibited broad absorption in the visible region and the tails extending to longer wavelengths. The band gap energy of the samples are measured by the extrapolation of the linear portion of the graph between the modified Kubelka-Munk function  $(F(R)hv)^2$  versus photon energy ( $hv$ ), as shown in Fig. 6(a) and 6(b) for CZTS and ZnO respectively. It is found that the band gaps of the CZTS sample is 1.53 eV. For designing a highly efficient solar cell, the band gap of the material that maximizes absorption of incident light is highly desirable and should be in the order of 1.3-1.5 eV<sup>[24]</sup>. Conversion efficiency of 3.03% has been reported by Feng Jiang *et al*<sup>[25]</sup> for CZTS thin film with a band gap 1.5eV. It is also reported that the values of band gap for CZTS nanocrystals with diameter ranging from 11 nm to 3 nm are 1.48 eV to 1.89 eV respectively<sup>[26]</sup>. In the present work, band gap value 1.53 eV was observed for the particle size 7 nm. The spectrum Fig. 5(b) reveals a maximum absorption at 325 nm for the ZnO sample. It was found that the bandgap of ZnO sample was 3.42eV and is in agreement with that of the earlier reports<sup>[27, 28]</sup>. The band gap values for ZnO and CZTS nanoparticles are quite close to the optimum band gaps required for buffer and absorber layers, respectively in solar cells.



**Fig. 6. Plot of  $(F(R)hv)^2$  versus  $(hv)$  of (a) CZTS and (b) ZnO nanoparticles**

### J-V Characteristics



**Fig. 7. J-V curve of CZTS/ZnO solar cell**

The current density voltage (J-V) characteristics of SLG/CZTS/ZnO/Al:ZnO/Al solar cell is shown in Fig. 7 and this has been measured under the light intensity of  $100 \text{ mW cm}^{-2}$  (AM1.5G). The solar cell exhibited the conversion efficiency ( $\eta$ ) of 2.37 % with fill factor (FF) = 50.84 %, open circuit voltage ( $V_{oc}$ ) = 0.44 V, short circuit current density ( $J_{sc}$ ) =  $10.54 \text{ mA/cm}^2$ , series resistance ( $R_s$ ) =  $9.19 \Omega \text{ cm}^2$  and shunt resistance ( $R_{sh}$ ) =  $154.14 \Omega \text{ cm}^2$ . Higher  $V_{oc}$  in the CZTS/ZnO cell could be considered as a benefit of utilizing wider band gap ZnO that might induce the formation of a higher built-in potential. On the other hand, the lower  $J_{sc}$  could be related with the recombination of minority carriers that is enhanced by the defects at CZTS/ZnO interface<sup>[10]</sup>.

### Conclusion

CZTS and ZnO nanoparticles were synthesized by a simple solvothermal method. The XRD results reveal that the CZTS and ZnO nanoparticles are kesterite and hexagonal crystalline in nature with the particle size of 7 nm and 13 nm. Raman analysis confirms the formation of single phase CZTS and ZnO nanoparticles. The SEM micrograph shows that the CZTS particles are homogeneous in nature and ZnO sample possess uniform hexagonal structures. The CZTS/ZnO heterojunction solar cell exhibited the photovoltaic performance with  $\eta$  of 2.37 % and FF of 50.84 %. This result suggests that ZnO can be an attractive Cd-free buffer candidate for CZTS based solar cells.

### References

1. Zhou H, Hsu WC, Duan HS, Bob B, Yang W, Song TB, Hsu CJ, Yang Y, CZTS nanocrystals: a promising approach for next generation thin film photovoltaics. *Energy Environ. Sci.*, 2013, 6, 2822-2838.
2. Chernomordik BD, B'eland AE, Trejo ND, Gunawan AA, Deng DD, Mkhoyan KA, Aydil ES, Rapid facile synthesis of  $\text{Cu}_2\text{ZnSnS}_4$  nanocrystals. *J. Mater. Chem. A*, 2014, 2, 10389-10395.
3. Sun L, He J, Kong H, Yue F, Yang P, Chu J, Structure, composition and optical properties of  $\text{Cu}_2\text{ZnSnS}_4$  thin films deposited by pulsed Laser deposition method. *Sol. Energy. Mater. Sol. Cells*, 2011, 95, 2907-2948.
4. Schubert BA, Marsen B, Cinque S, Unold T, Klenk R, Schorr S, Schock HW,  $\text{Cu}_2\text{ZnSnS}_4$  thin film solar cells by fast coevaporation, *Prog. Photovolt. Res. Appl.*, 2011, 19, 93-96.
5. Kannan AG, Manjulavalli TE, Chandrasekaran J, Influence of solvent on the properties of CZTS nanoparticles. *Procedia Engineering*, 2016, 141, 15-22.



6. Annapoornam Ganesan Kannan, Thirumalaisamy Esvaramoorthy Manjulavalli, Synthesis and characterization of  $\text{Cu}_2\text{ZnSnS}_4$  nanoparticles. *Nanomaterials and Energy*, 2015, 4(NME2), 118-123.
7. KannanAG, Manjulavalli TE, Characterization of CZTS Nanoparticles Synthesized by Solvothermal Method for Solar Cell Application. *Int.J. ChemTech Res.*,2015, 7(3)1167-1171.
8. Byungha Shin, Oki Gunawan, Yu Zhu, Nestor A. Bojarczuk, S. Jay Chey, SupratikGuha, Thin film solar cell with 8.4% power conversion efficiency using an earth-abundant  $\text{Cu}_2\text{ZnSnS}_4$  absorber. *Progress in Photovoltaics*, 2013, 21(1), 72-76.
9. WujisigulengBao, Masaya Ichimura, Band Offsets at the  $\text{ZnO}/\text{Cu}_2\text{ZnSnS}_4$  Interface Based on the First Principles Calculation. *Japanese Journal of Applied Physics*, 2013, 52, 061203-(1-5).
10. Htay MT, Hashimoto Y, Momose N, Sasaki K, Ishiguchi H, Igarashi S, Sakurai K, Ito K, A Cadmium-Free  $\text{Cu}_2\text{ZnSnS}_4/\text{ZnO}$  Hetrojunction Solar Cell Prepared by Practicable Processes. *Jpn. J. Appl. Phys.* 2011, 50, 032301.
11. Katagiri H, Jimbo K, Tahara M, Araki H, Oishi K, The Influence of the Composition Ratio on CZTS-based Thin Film Solar Cells. *MRS Proc.*,2009, 1165, M04-01.
12. Nithya R, Kannan AG, Manjulavalli TE, Investigation of Pure and Transition Metal Doped ZnO Nanoparticles for Photovoltaic Applications. *Int.J. ChemTech Res.*, 2015, 7(3) 1178-1184.
13. PalMou, Mathews NR, Gonzalez R, Silva, Mathew X, Synthesis of  $\text{Cu}_2\text{ZnSnS}_4$ nanocrystals by solvothermal method. *Thin Solid Films*, 2013, 535, 78-82.
14. Bao D, Gu H, Kuang A. Sol-gel-derived c-axis oriented ZnO thin films. *Thin solid films*, 1998, 312(1-2), 37-39.
15. Zhang Y, Lin B, Fu Z, Liu C, Han W, Strong ultraviolet emission and rectifying behavior of nanocrystallineZnO films. *Opt. Mater.*, 2006, 28, 1192-1196.
16. Sousa MG, Cunha AF, Fernandes PA, Teixeira JP, Sousa RA, Leitão JP, Effect of rapid thermal processing conditions on the properties of  $\text{Cu}_2\text{ZnSnS}_4$  thin films and solar cell performance. *Sol. Energy Mater. Sol. Cells.*, 2014, 126, 101-106.
17. Tiwari D, Chaudhuri TK, Rayb A, Tiwaric KD,  $\text{Cu}_2\text{ZnSnS}_4$  thin films by simple replacement reaction route for solar photovoltaic application. *Thin Solid Films*, 2014, 551, 42-45.
18. Kheraj V, Patel KK, Patel SJ, Shah DV, Synthesis and characterisation of Copper Zinc Tin Sulphide (CZTS) compound for absorber material in solar-cells. *Journal of Crystal Growth*,2013, 362, 174-177.
19. Dalapati GK, Batabyal SK, Masudy-Panah S, Su Z, Kushwaha A, Wong TI, Liu HF, Bhat T, Iskander A, Lim Y, Wong LH, Tripathy S, Chi D, Sputter grown sub-micrometer thick  $\text{Cu}_2\text{ZnSnS}_4$  thin film for photovoltaic device application. *Materials Letters*, 2015, 160, 45-50.
20. VipulKheraj, Patel KK, Patel SJ, Shah DV, Synthesis and characterisation of Copper Zinc Tin Sulphide (CZTS) compound for absorber material in solar-cells.*Journal of Crystal Growth*, 2013, 362, 174–177.
21. Khan A. Alim, Vladimir A. Fonoberov, Manu Shamsa, and Alexander A. Balandina, Micro-Raman investigation of optical phonons in ZnOnanocrystals.*Journal of Applied Physics*, 2005, 97, 124313.
22. Pradhan AK, Kai Zhang, Loutts GB, Roy UN, Cui Y, Burger A, Structural and spectroscopic characteristics of ZnO and  $\text{ZnO}:\text{Er}^{3+}$  nanostructures. *J. Phys.: Condens. Matter*, 2004, 16, 7123-7130.
23. Tauc J, Grigorovici R, Vancu A, Optical properties and electronic structure of amorphous germanium.*Physica Status Solidi B.*,1966, 15, 627–637.
24. Zachary DP, Henkelman G, Hybrid density functional theory band structure engineering in hematite. *The journal of chemical physics*,2011, 134, 224706-(1-9).
25. FengJianga, HonglieShen, Fabrication and photovoltaic properties of  $\text{Cu}_2\text{ZnSnS}_4/\text{i-a-Si}/\text{n-a-Si}$  thin film solar cells. *Applied Surface Science*, 2013, 280, 138–143.
26. Liu WC, Guo BL, Wu XS, Zhang FM, Mak CL, Wong KH, Facile hydrothermal synthesis of hydrotropic  $\text{Cu}_2\text{ZnSnS}_4$ nanocrystal quantum dots: band-gap engineering and phonon confinement effect. *J Mater Chem A.*, 2013, 1, 3182–3186.
27. Geetha MS, Nagabhushana H, Shivananjaiiah HN, Green mediated synthesis and characterization of ZnO nanoparticles using Euphorbia Jatropa latex as reducing agent. *Journal of Science: Advanced Materials and Devices*, 2016, 1(3), 301–310.
28. VioricaMuşat, AurelTăbăcaru, BogdanŞtefanVasile, Vasile-Adrian Surdu, Size-dependent photoluminescence of zinc oxide quantum dots through organosilane functionalization. *RSC Adv.*, 2014, 4, 63128-63136.

\*\*\*\*\*